

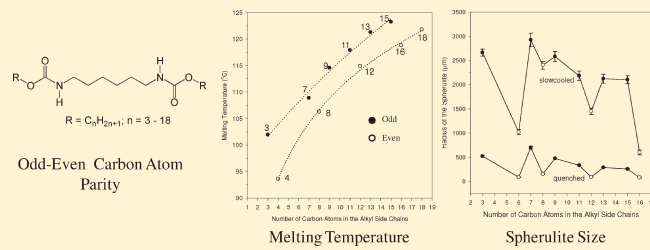
Effects of Carbon Atom Parity and Alkyl Side Chain Length on the Crystallization and Morphology of Biscarbamates, A Set of Model Compounds for Polyurethanes

Mostafa Kamal Khan and Pudupadi R. Sundararajan*

Department of Chemistry, Carleton University, 1125 Colonel By Drive, Ottawa, Ontario K1S 5B6, Canada

Supporting Information

ABSTRACT: Solid state morphology and crystallization behavior of a homologous series of biscarbamate molecules having varying alkyl side chain lengths with different carbon atom parity were investigated. These are model compounds for polyurethanes. We synthesized a set of biscarbamates with double hydrogen bonding motifs separated by a $(\text{CH}_2)_6$ spacer and with alkyl side chains of various lengths ranging from C_3 to C_{18} at the ends. Thermal analysis showed an odd–even alternation in their melting temperatures and heats of fusion, with the odd number of carbon atoms in the side chain having higher melting temperatures and heats of fusion than the even numbered ones, in contrast to the case of n -alkanes. The effect of carbon atom parity in the alkyl side chains on the spherulite size, spherulite growth rate, and isothermal crystallization kinetics was studied. Although the spherulite size increases with the alkyl side chain length, the maximum is seen at an intermediate length and not with a short or long alkyl chain for both the odd and even series. Along this series of molecules, a maximum in spherulite size, spherulite growth rate, and rate of crystallization is seen for C_7C_6 (odd series) and C_8C_6 (even series) biscarbamates. There is a significant difference in spherulite size with respect to carbon atom parity in the alkyl side chains as well as sample preparation protocol. Hence the length of the alkyl side chain, carbon atom parity in the alkyl side chains, and the sample preparation protocol (i.e., quenching versus slow cooling) play an important role in the morphology of these molecules. We rationalize this behavior with the relative contributions of hydrogen bonding and van der Waals forces as discerned from IR spectroscopy. While the van der Waals interaction increases with the alkyl side chain length in this series, the hydrogen bond contribution remains invariant. The rate of crystallization follows the trend seen with the spherulitic growth. The Avrami exponent is significantly smaller than 3, varying from 1.6 to 2.5 depending on the side chain length, which indicates that the crystallization is not truly three-dimensional. This study on the influence of alkyl side chains shows that while hydrogen bonding enables self-assembly the van der Waals interactions play a significant role in the crystallization and morphology of such self-assembled structures.



INTRODUCTION

Molecular self-assembly mediated by noncovalent interactions such as hydrogen bonding, dispersion forces, $\pi-\pi$ interactions, etc. has long been studied and emerged as a powerful tool for creating supramolecular architectures of desired dimensions and functionality.¹ This toolbox offers a “bottom-up” and in fact the only practical approach for producing a variety of structures at multiple length scales.² Among the various noncovalent interactions, hydrogen-bond-mediated self-assembly has been extensively studied in recent years and employed to create specific secondary structures with oligomers,³ molecular strands employed in specific modes of intermolecular aggregates,⁴ etc. The effectiveness of hydrogen bonding in such molecular self-assembly depends largely on the design of tailored recognition elements in the form of hydrogen-bond donor–acceptor arrays.⁵ While the appropriate design of molecules with hydrogen bonding moieties leads to molecular self-assembly, the morphology of the structures created by such an assembly was found to be

dependent on the secondary noncovalent interactions such as van der Waals forces.^{6,7} In many cases the length and carbon atom parity in the alkyl spacer or side chains play an important role in such secondary interactions leading to an “odd–even” effect on the molecular packing, morphology, and subsequent physical properties.

The odd–even effect of the carbon number parity of methylene groups in aliphatic chains is a well-known and an extensively studied phenomenon.⁸ This effect has been observed in the solid state,⁹ solution phases,¹⁰ and solid/liquid interfaces¹¹ and has been mainly attributed to packing differences in the crystal structures¹² between chains having odd or even numbers of carbon atoms. Although liquid crystals,¹³ as a class of molecules, are known to exhibit such an odd–even effect, others, e.g., polyurethanes,¹⁴

Received: April 24, 2011

Revised: June 7, 2011

Published: June 08, 2011

Scheme 1

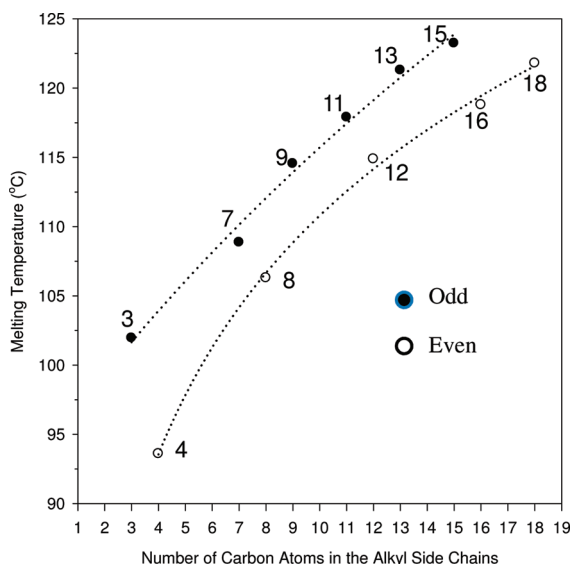
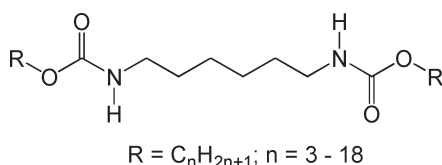


Figure 1. Variation of melting temperature of the biscarbamates with the number of carbon atoms in the alkyl side chains.

n-alkanes,¹⁵ carboxylic acids,¹⁶ alcohols,¹⁷ bifunctional hydroxy-carboxylic acids,¹⁸ etc., also show the odd–even effect as a function of carbon atom parity. In the overwhelming majority of the literature, this effect is discussed with respect to the carbon atom parity in the spacer groups.¹⁹ However, there are some reports where this effect is discussed as a function of the carbon atom parity in the alkyl side chains.²⁰ In most of the cases, the odd–even effect is manifested in the phase transition temperatures^{13b} and optical properties^{13c} of such compounds. In this paper we discuss the significant differences in the crystallization and morphological behavior of a class of self-assembling molecules, namely, biscarbamates (model compounds for polyurethanes), as a function of the carbon atom parity in the alkyl side chains symmetrically attached to the hydrogen bonding moieties (Scheme 1).

Scientific studies of this class of molecules date back to the early 1900s and continue to the contemporary time because of their potential applications as sequence-specific DNA alkylation agents,²¹ organic intermediates,²² photosynthetic inhibitors,²³ models for alcohol prodrugs,²⁴ efficient and nontoxic gene delivery systems,²⁵ and antileukemic agents,²⁶ etc. Because of their structural similarity, carbamates and biscarbamates are considered model compounds for polyurethanes, and the mechanism of decomposition²⁷ and surface adhesion²⁸ of polyurethanes has been studied in terms of those of biscarbamates. Moreover, they have been used in improving hardness of polyurethane-based adhesives and sealants,²⁹ adjusting the viscosity of oil and grease and as anti-inflammatory agents,³⁰ and pesticides.³¹ Because of their low melt viscosity of about 8–12 cPs and melting temperatures

Scheme 2

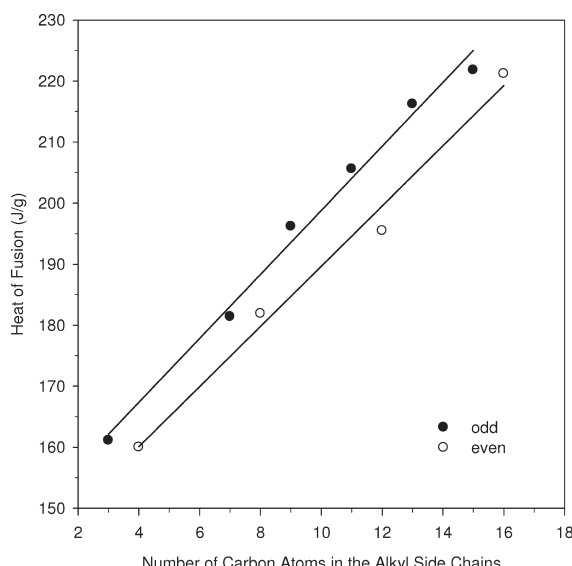
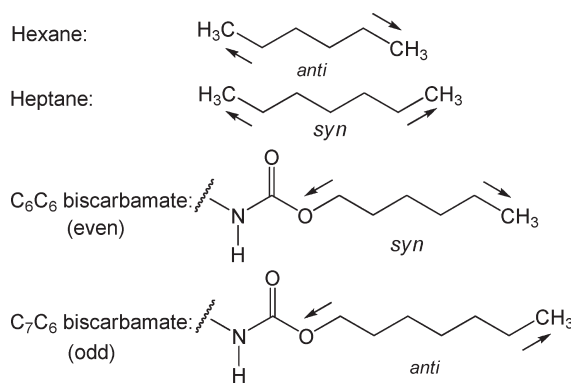


Figure 2. Change of heat of fusion of the biscarbamates with the number of carbon atoms in the alkyl side chains.

of 60–120 °C, carbamates and biscarbamates have been considered as potential candidates as an ink vehicle for inkjet printing technologies since they also crystallize rapidly upon quenching from the melt.³²

In our previous publications, we compared the morphology and thermal behavior of *N*-octadecyl carbamates referred to therein as monocarbamates⁶ and biscarbamates⁷ with alkyl side chains of various lengths ranging from *C*₄ to *C*₁₈ with an even carbon atom parity in the side chains. We observed significant differences in their morphology and thermal properties which were attributed to the influence of single versus double hydrogen bonding motifs as well as asymmetric versus symmetric alkyl substitution. In sharp contrast to the monocarbamates, biscarbamates with an alkyl side chain length of *C*₈ showed the maximum spherulite size, spherulite growth rate, and rate of crystallization. These observations were rationalized on the basis of the relative contributions of hydrogen-bond and van der Waals forces. In another publication,³³ we showed that the biscarbamates show immiscibility and molecular selectivity at the molecular level upon blending. A preliminary study^{7b} on the gelation behavior of these biscarbamates showed a significant difference in their gel

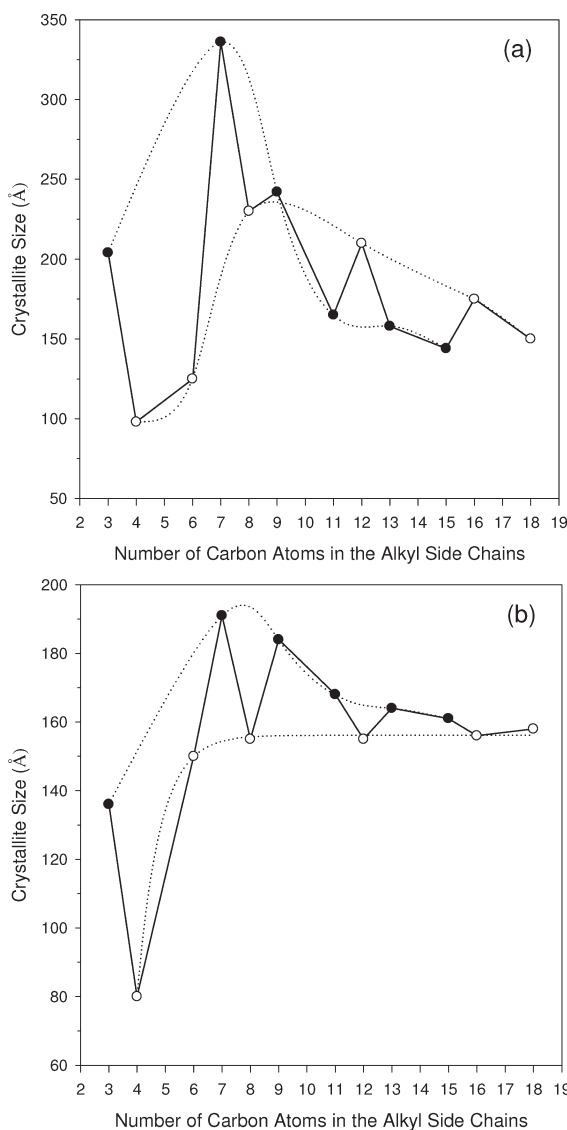


Figure 3. Variation in crystallite size of biscarbamates with odd and even numbers of carbon atoms in the alkyl side chains for d -spacing (a) 3.5 and (b) 4.3 \AA reflections.

state morphology depending on their carbon atom parity in the alkyl side chains. On the basis of these observations, we believed that it would be of interest to study the crystallization behavior of these materials in the solid state as a function of the carbon atom parity in the alkyl side chains. To this end, we synthesized a series of biscarbamates with both an odd and even number of carbon atoms in the alkyl side chains and studied their morphology and crystallization behavior to compare them with respect to the carbon atom parity in the alkyl side chains.

EXPERIMENTAL SECTION

Biscarbamates containing odd and even numbers of carbon atoms in the alkyl side chains were synthesized as described by Goodbrand et al.³⁴ from the appropriate diisocyanate and alcohols.

Thermal analysis was performed using a TA Instruments 2010 differential scanning calorimeter at a heating rate of 10 $^{\circ}\text{C}/\text{min}$. The calorimeter was calibrated for temperature and energy with

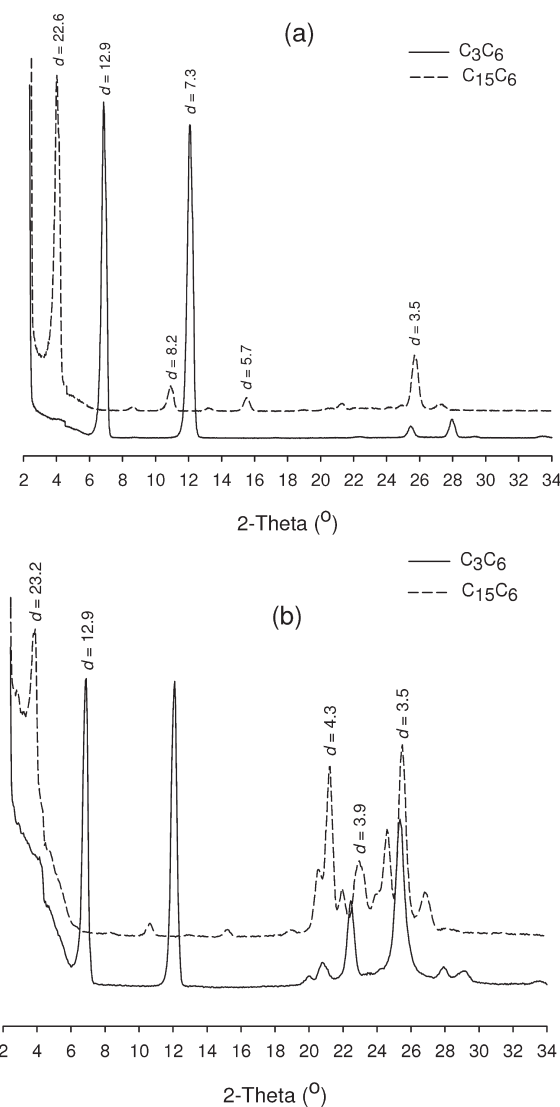


Figure 4. X-ray diffraction traces of (a) as-synthesized and (b) slow-cooled samples of C_3C_6 and C_{15}C_6 biscarbamates.

an indium sample as a standard reference material. DSC traces were recorded in a nitrogen atmosphere with 7–10 mg of the sample and using the Thermal Advantage software. The data were processed by TA Universal Analysis software. For isothermal crystallization studies, the samples were heated to a temperature about 40 $^{\circ}\text{C}$ above their melting points and then allowed to cool to a temperature 5 $^{\circ}\text{C}$ above their crystallization temperatures. The melt of the samples was then cooled to their crystallization temperature at a rate of 1 $^{\circ}\text{C}/\text{min}$ and allowed to stay at isothermal conditions for 30 min. The heat of crystallization was measured at 0.6 s intervals, and the crystallinity was determined by integrating the isothermal heat flow curve with respect to time. The fractional degree of crystallization (α) was calculated by the ratio of the heat of crystallization at time t to the total heat of crystallization using the following equation:

$$\alpha = \frac{\Delta H_t}{\Delta H_{\infty}} = \frac{\int_0^t \frac{dQ}{dt} dt}{\int_0^{\infty} \frac{dQ}{dt} dt} \quad (1)$$

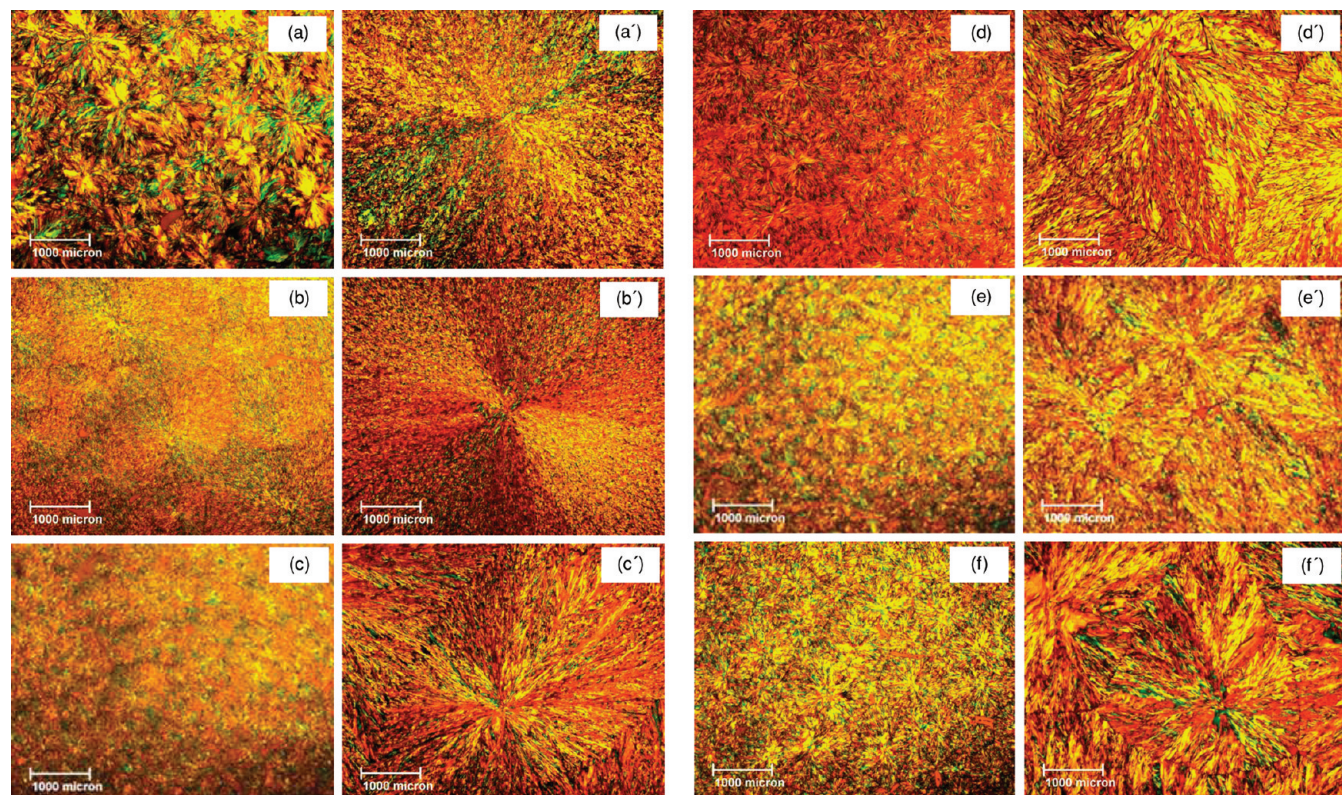


Figure 5. Optical micrographs of bis(alkyl carbamate)s with different odd numbers of carbon atoms in the alkyl side chains: (a, a') C_3 , (b, b') C_7 , (c, c') C_9 , (d, d') C_{11} , (e, e') C_{13} , and (f, f') C_{15} bis(alkyl carbamate)s. (a), (b), (c), (d), (e), and (f) represent the micrographs of quenched samples, and (a'), (b'), (c'), (d'), (e'), and (f') represent those of slow-cooled samples.

where ΔH_t is the partial area between the DSC curve and the time axis at time t and ΔH_∞ is the total area under the peak that corresponds to the total heat of crystallization.

The crystallization kinetics was studied using the Avrami equation³⁵ as follows

$$1 - X(t) = \exp(-Kt^n) \quad (2)$$

$$\ln\{-\ln[1 - X(t)]\} = \ln K + n \ln t \quad (3)$$

where $X(t)$ is the relative crystallinity; t is the crystallization time; n is the Avrami exponent; and K is the crystallization rate constant. Half crystallization time ($t_{1/2}$) that represents the crystallization rate can be obtained from the following equation

$$t_{1/2} = [\ln 2/K]^{1/n} \quad (4)$$

Optical micrographs were recorded on a Zeiss AxioPlan polarized optical microscope (POM). Northern Eclipse (version 8.0) image processing software was used to capture the images as well as to calculate the spherulite size. The samples for optical microscopy were prepared by melting a small amount of the material on a microscope slide at a temperature 20 °C above the corresponding melting temperature of the sample, holding it isothermally for 10 min to remove morphological history if there was any, and then cooling it slowly to room temperature at the rate of approximately 5 °C/min. Another set of samples was prepared following the same procedure but by quenching the samples immediately to room temperature from the melt instead of slow cooling. For the kinetic study of the spherulite growth, a Linkam hot stage LTS 350 equipped with a Linkam TMS 94

thermo-controller was used. The samples were heated to a temperature of 20 °C above the melting temperature of the bis(alkyl carbamate) at a rate of 5 °C/min and held at that temperature for about 10 min. The samples were then cooled at a rate of 2 °C/min to a temperature of 5 °C above the crystallization temperature (T_c) and then at the rate of 0.1 °C/min to the T_c . Northern Eclipse image processing software was used to capture the images at specific time intervals during the crystallization of the samples isothermally held at their T_c followed by the calculation of the spherulite size for subsequent data processing.

A Philips automated powder diffractometer (PW1710) with Ni-filtered $Cu K\alpha$ radiation ($\lambda = 1.5418 \text{ \AA}$) was used for X-ray diffraction studies. The samples for XRD studies were prepared by melting them on the glass slide and then either slowly cooling or quenching them to room temperature. Possible orientation of the molecular aggregates was checked by recording additional XRD traces by rotating the sample holder at 90° in the measurement plane. Diffraction traces were recorded at ambient temperature in the range of $2^\circ \leq 2\theta \leq 45^\circ$ using MDI DataScan 3.2 (Materials Data Inc., Livermore, CA) software. The XRD traces were processed, and the results were analyzed using the MDI Jade 5.0 XRD pattern processing software. The crystallite size, L , corresponding to a particular reflection was calculated using the Scherrer equation:³⁶

$$L = K\lambda/\beta \cos \theta \quad (5)$$

where λ is wavelength of the X-ray; θ is half the scattering angle; and β is the full width at half-maximum of the peak on the 2θ scale in radians; $K = 0.9$.

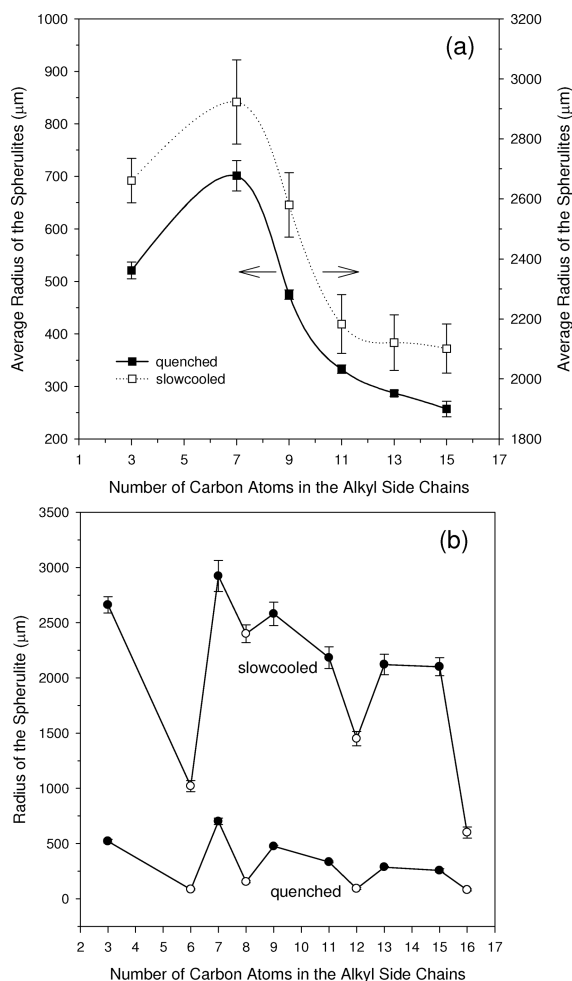


Figure 6. (a) Variation of spherulite size of C_xC_6 biscarbamates with alkyl side chains containing odd numbers of carbon atoms. The right ordinate corresponds to the slow-cooled samples. (b) Results for both odd and even numbers of carbon atoms.

FTIR spectra of the pure biscarbamates were recorded under ambient conditions with a Varian 1000 Scimitar Series spectrophotometer, by preparing the samples with KBr pellets. A background correction was performed using an identical blank KBr pellet. For comparison, FTIR spectra of the same set of samples were taken under ambient conditions with the same spectrophotometer in attenuated total reflectance (ATR) mode. The FTIR spectra were recorded with MIRacle single reflection ATR accessories from Pike Technologies (Madison, WI) with a background correction using the identical sample holder. The data were processed using the Varian Resolution (version 4.0.5.009) spectra processing software. We did not see any difference between the normal transmission and ATR modes, and the data presented here are of ATR mode.

RESULTS AND DISCUSSION

Thermal Behavior. We denote the samples as C_xC_6 , where x corresponds to the number of carbon atoms in the alkyl side chain and 6 refers to the $(CH_2)_6$ spacer. The melting temperatures of both odd and even biscarbamates as a function of number of carbons in the alkyl side chains are plotted in Figure 1. Two representative DSC traces of C_3C_6 (odd) and C_4C_6 (even)

biscarbamates are shown in Figure S1 (Supporting Information), showing the phase transitions corresponding to their melting and crystallization. The appearance of sharp peaks without any other transitions prior to both their melting and crystallization implies high purity and the absence of any polymorphism. The numerical values of T_m are listed in Table S1 (Supporting Information). It is seen from Figure 1 that biscarbamates of this series show odd–even oscillation of melting temperatures with higher T_m for a molecule with an odd number of carbon atoms than the molecule containing the next consecutive even number. The difference is more pronounced with the shorter side chains. The T_m of C_3C_6 biscarbamate is $102\text{ }^\circ\text{C}$, while that of C_4C_6 is $91.3\text{ }^\circ\text{C}$ with a difference of $\sim 11\text{ }^\circ\text{C}$. However, the difference between the melting temperatures of $C_{15}C_6$ and $C_{16}C_6$ is only $4.4\text{ }^\circ\text{C}$. Among this series of molecules, we see the least difference in T_m between C_7C_6 and C_8C_6 which is only $2.3\text{ }^\circ\text{C}$. While the odd–even effect is less pronounced with an increase in the alkyl side chain length, the least odd–even effect in T_m is seen between C_7C_6 and C_8C_6 which show the maximum crystallization rate and spherulite size (discussed in the following sections) among the members of the biscarbamates containing odd and even numbers of carbon atoms.

The odd–even effect of carbon atom parity on thermal properties seen here is different from the trend reported for *n*-alkanes. Boese et al.¹² noted that *n*-alkanes having an even number of carbon atoms have higher melting temperatures than those of odd numbered alkanes. The even numbered *n*-alkanes are centrosymmetric, and the odd numbered ones are C_2 symmetric. As shown in Scheme 2, in the case of hexane, the terminal methyl groups are pointing in opposite directions (*anti*), and those of heptane are in the same direction (*syn*). This leads to differences in the packing of terminal methyl groups in the crystal structures of these molecules. The even-numbered *n*-alkanes have symmetrical intermolecular contacts at both ends, whereas the odd numbered ones have a longer distance of contact at one end.¹² A different trend in odd–even effect is seen with the biscarbamates studied here. Biscarbamates with an odd number of carbon atoms show higher melting temperatures and heat of fusion than the even numbered. By analogy to the *n*-alkanes shown in Scheme 2, we note that the terminal methyl group is disposed in a direction opposite to the ester oxygen in C_7C_6 (*anti*, similar to the terminal methyl groups in hexane), whereas both the ester oxygen and the terminal CH_3 group are in the same direction with C_6C_6 (*syn*, similar to the case of heptanes in Scheme 2).

Such a *syn* disposition is also seen in the crystal structure³⁷ of $C_{10}C_6$. Inherent differences of this nature in the molecular structure would lead to different packing modes of the odd and even series. On the basis of the analogy with *n*-alkanes, we speculate that hydrogen bonding in consonance with dispersion forces leads to a more dense packing of biscarbamates with odd numbered carbon atoms in the side chain than the even numbered biscarbamates.

Contrary to this trend, we see a less pronounced odd–even effect on the heats of fusion (ΔH) of these biscarbamates. Figure 2 shows that the ΔH of the series containing both odd and even numbers of carbon atoms increases linearly with the alkyl side chain length. We do not see any significant difference in the heat of fusion of two biscarbamates containing a successive odd and even number of carbon atoms in extreme lengths of alkyl side chains. However, there is a significant difference in ΔH between two biscarbamates with intermediate alkyl side chain lengths. For example, the difference in ΔH is only 1.1 and 0.6 J/g between the C_3C_6/C_4C_6 and $C_{15}C_6/C_{16}C_6$ odd–even pairs,

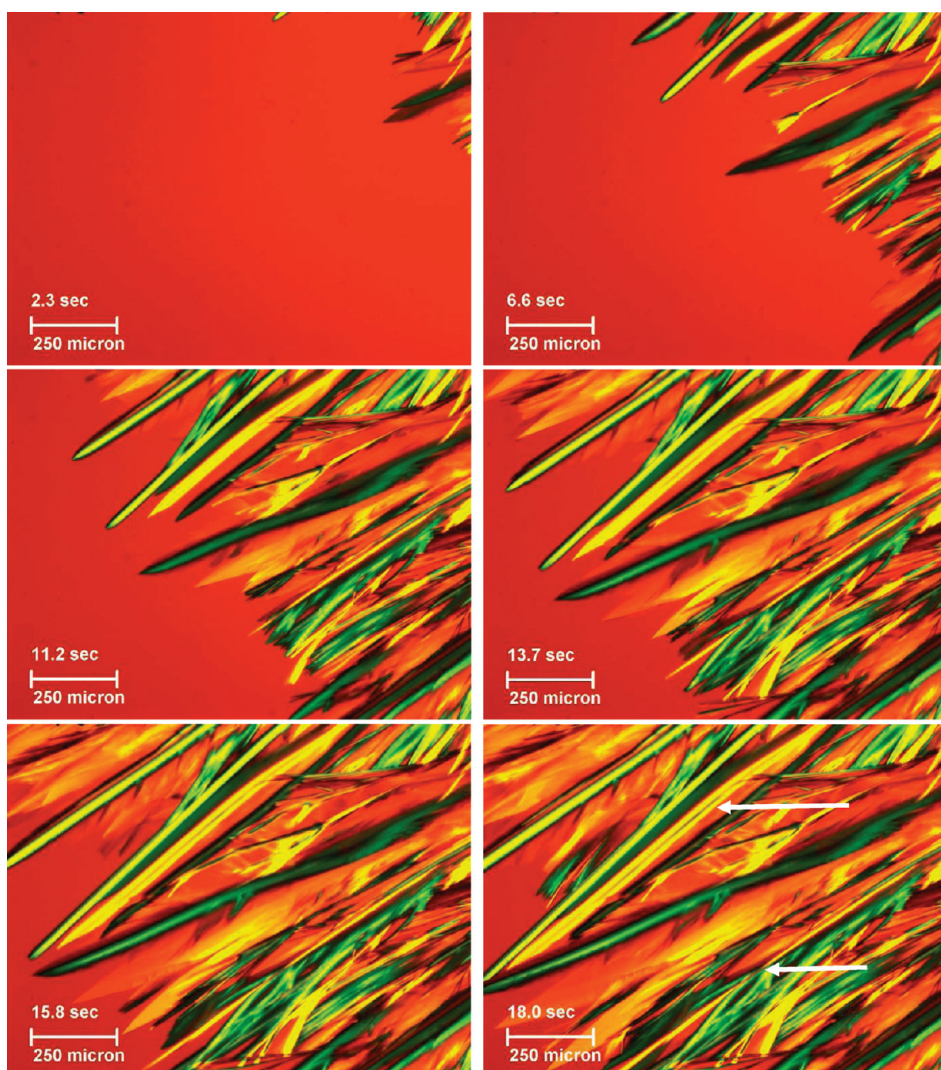


Figure 7. Optical micrographs of $C_{13}C_6$ bismcarbamate recorded at different time intervals during isothermal spherulite growth. The arrows point to the eaves trough morphology.

respectively. On the other hand, the difference in ΔH is 10.1 J/g between $C_{11}C_6$ and $C_{12}C_6$ bismcarbamates.

X-ray Diffraction and Structural Features. The crystal structure of the $C_{10}C_6$ molecule was found to be triclinic with a center of symmetry.³⁷ To our knowledge, crystal structures have not been reported for the other bismcarbamates studied here. Crystalline conformations of polyurethanes with a C_6 spacer between the hydrogen bonding moieties have been reported.³⁸ On the basis of X-ray powder diffraction data, we note a few structural features, similar to those in the above-mentioned studies. We did not see any significant difference between the corresponding peak positions of quenched and slow-cooled samples, which indicates that molecular packing of these molecules is independent of sample preparation procedure (i.e., quenching or slow cooling). Two reflections with d -spacings of ~ 4.3 and 3.5 \AA were common to all the samples studied here. These reflections were observed at 4.6 and 3.8 \AA in the case of even C_xC_6 bismcarbamates. Using the same packing mode as in the above crystallographic studies, the 4.3 \AA reflection is assigned to the (001) plane,³⁷ and it is the distance between the molecules in the H-bonding plane. The 3.5 \AA reflection corresponds to the (010)

plane, and it is the distance between the H-bonding planes (see Figure 4 of ref 7a). Note that in the crystallographic studies on the polyurethanes³⁸ the length of the molecule corresponds to the c -axis of the unit cell.

The spherulitic morphology (*see the next section*) develops upon crystallization from the melt, and the growth directions of the molecules in the lamellae of the spherulites were discussed before.^{7a} It was shown that the radial direction of the lamellae of the spherulites corresponds to the hydrogen bonding direction (the 4.3 \AA reflection) and that the stacking of these hydrogen bonded planes is in the tangential direction (the 3.5 \AA reflection). The average size of the crystallites along these two growth directions can be determined using the half-width of the diffraction peaks corresponding to these reflections and the Scherrer equation³⁶ (eq 5). Figure 3 shows the variation of crystallite size of the reflections at $d = 3.5$ and 4.3 \AA as a function of the alkyl side chain length of quenched samples, for both odd and even C_xC_6 bismcarbamates. It is seen that the crystallite size with $d = 3.5 \text{ \AA}$ increases sharply with the increase in alkyl chain length from C_3 to C_7 and decreases significantly with further increase. This observation conforms to the variation of spherulite size and rate

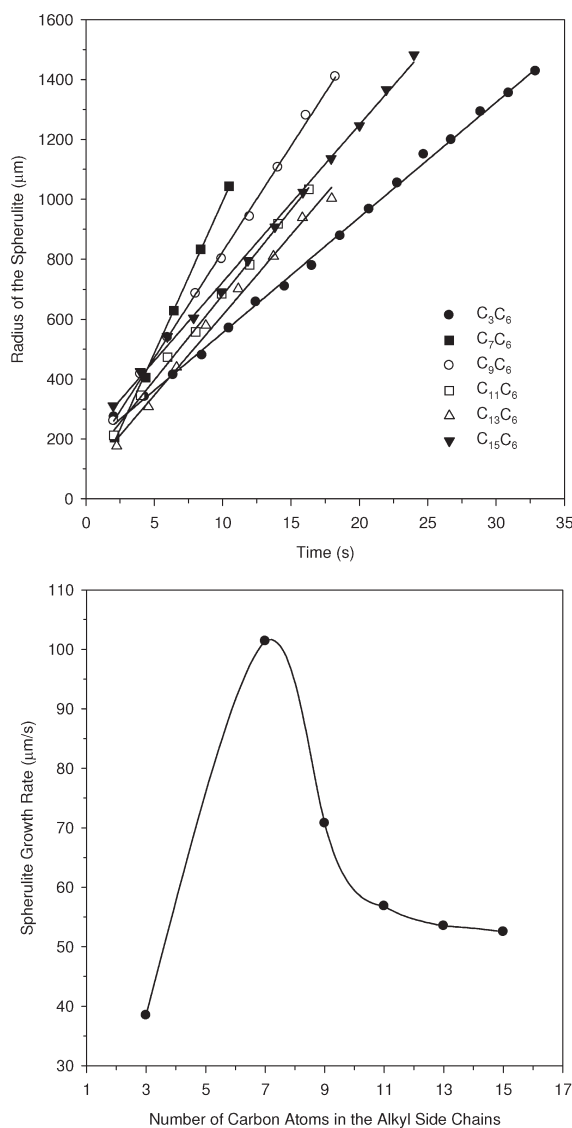


Figure 8. (a) Growth of spherulites with time and (b) rate of spherulite growth as a function of number of carbon atoms in the alkyl side chains.

of crystallization of these molecules (*see below*). A similar trend is seen for the reflection at $d = 4.3 \text{ \AA}$ although the extent of variation is small. A comparison of crystallite sizes of the corresponding reflections of both the odd and even biscarbamates shows that odd biscarbamates show larger crystallite size than the corresponding even biscarbamates.

Another feature that is seen commonly among the biscarbamates with even and odd alkyl side chains is that apart from the high intensity reflection with the large d -spacing (which corresponds to the (100) direction of the unit cell³⁷) most of the other reflections are weak, as seen in Figure 4 for the as-synthesized and slow-cooled samples of C_3C_6 and $C_{15}C_6$. This effect is pronounced with the longer side chains. This indicates predominant stacking along one direction.

Morphology. Figure 5 shows the cross polarized optical micrographs of the quenched (left) and slow-cooled (right) samples of the corresponding C_xC_6 biscarbamates. The C_3C_6 biscarbamate having the lowest number of carbon atoms studied in this series shows well-defined spherulitic morphology for both

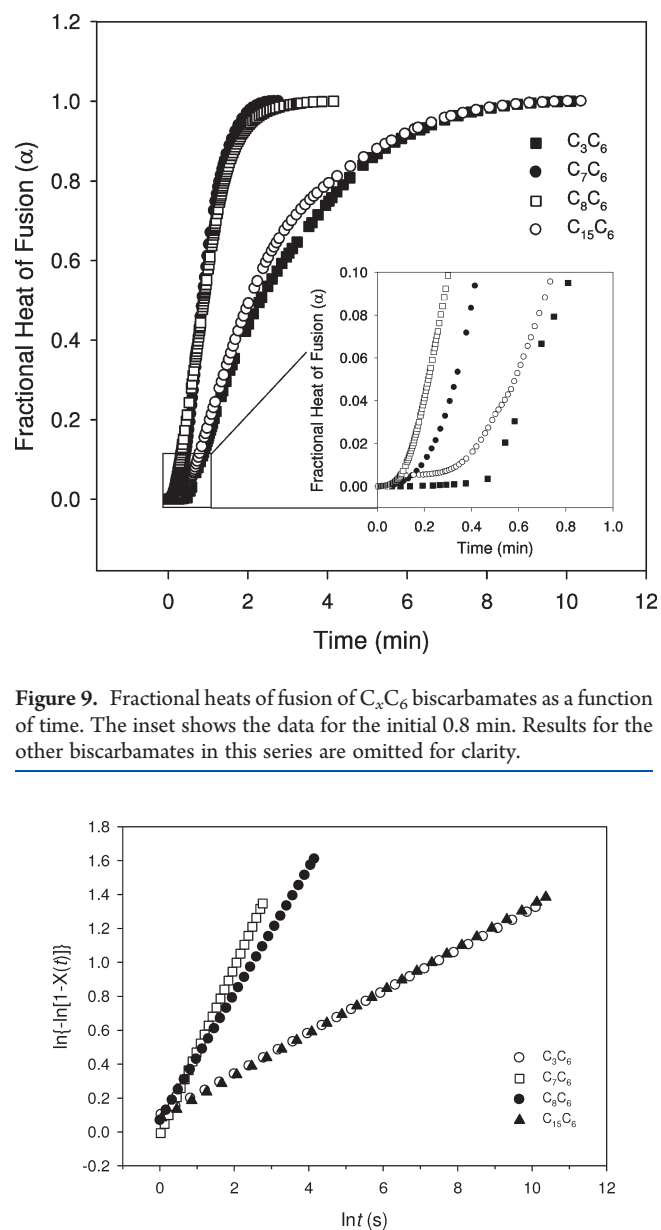


Figure 9. Fractional heats of fusion of C_xC_6 biscarbamates as a function of time. The inset shows the data for the initial 0.8 min. Results for the other biscarbamates in this series are omitted for clarity.

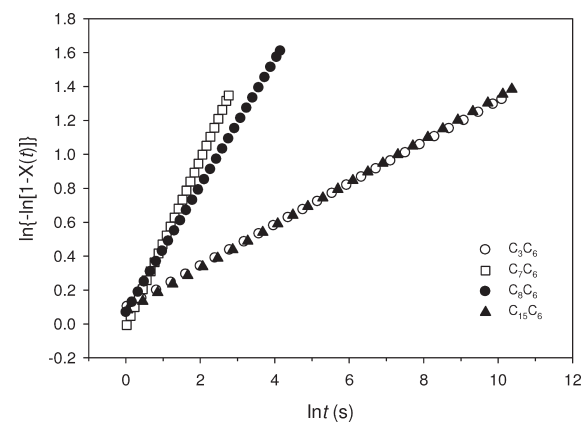


Figure 10. Plots of $\ln\{-\ln[1 - X(t)]\}$ versus $\ln t$ during isothermal crystallization of the biscarbamates. Data for other biscarbamates in this series are omitted for clarity.

quenched and slow-cooled samples. This is in contrast to the morphological behavior of the corresponding C_4C_6 biscarbamate which showed no spherulitic morphology for either quenched or slow-cooled sample.

It is seen from Figure 5, as expected, that the slow-cooled samples of these biscarbamates form larger spherulites than those of quenched samples upon crystallization. Figure 6a shows the variation of the spherulite size with respect to the alkyl side chain length for both quenched and slow-cooled samples. Spherulite size of these biscarbamates increases, like their even numbered counterparts, from C_3C_6 to C_7C_6 with an increase in the alkyl side chain length and then drastically decreases up to C_{11} chain length and more slowly thereafter. Fewer nucleation sites in the samples result in larger spherulites. The variation in nucleation site density and of spherulite size with respect to the alkyl side

Table 1. Isothermal Crystallization Parameters Calculated Using the Avrami Equations and the Corresponding Avrami Plots

sample	slope (n)	intercept ($\ln K$)	K	$\ln 2/K$	$1/n$	$t_{1/2}$ (s)
C_3C_6	1.916	-8.74	1.60×10^{-4}	4332	0.5218	79
C_7C_6	2.579	-10.24	3.56×10^{-5}	19470	0.3877	46
C_9C_6	2.215	-9.28	9.33×10^{-5}	7429	0.4515	56
$C_{11}C_6$	1.89	-8.07	3.12×10^{-4}	2221	0.5291	59
$C_{13}C_6$	1.639	-7.35	6.41×10^{-4}	1081	0.6101	71
$C_{15}C_6$	1.935	-8.86	1.41×10^{-4}	4916	0.5169	81

chain length can be rationalized with the relative contribution of H-bonding and van der Waals interactions of the molecules. Increased intermolecular association is expected to contribute to increased nucleation site density and hence to reduction in the spherulite size. This rationale can be explained with infrared spectroscopy of these biscarbamates. Figure 6b shows the change in spherulite size of biscarbamates with both odd and even numbers of carbon atoms. An odd–even oscillation in spherulite size is also seen in this case which parallels such variations of melting temperatures and heats of fusion.

Spherulite Growth Rate. The effects of odd versus even numbers of carbon atoms and the length of alkyl side chains on the crystallization of these molecules were further investigated with isothermal spherulite growth kinetics using hot-stage microscopy as described in the Experimental Section. Figure 7 shows the micrographs of $C_{13}C_6$ recorded at different times of spherulite formation from such an experiment. Because of the very fast growth of spherulite, we could not capture the images right at the beginning of the formation of the spherulites centering at the point of nucleation. It is seen from the micrographs that spherulite grows radially with extensive sequential branching of the lamellae over time. They also appear feather-like, often with a trough, as indicated by the arrows. The variation of the size of the spherulites as a function of time is shown in Figure 8a. It is seen that the spherulite growth is complete due to impinging of the adjacent spherulites within 10 s for C_7C_6 , while it takes about 33 and 24 s for C_3C_6 and $C_{15}C_6$, respectively. Thus, biscarbamates with extreme alkyl side chain length show slower spherulite growth rate than that of biscarbamates with intermediate side chain length. None of these plots extrapolate to a spherulite size of zero at $t = 0$ s, indicating a very fast growth of spherulites at the beginning. Figure 8b shows the spherulite growth rate as a function of alkyl side chain length. It increases from C_3C_6 to C_7C_6 and decreases significantly with the increase in the alkyl side chain length. Along this series of biscarbamates, C_7C_6 shows the maximum growth rate. This observation is in accord with the change in spherulite size of these molecules with respect to the alkyl side chain length. A comparison of spherulite growth rates of biscarbamates with alkyl side chains containing odd and even numbers of carbon atoms shows that odd biscarbamates have slower growth rate than the even carbon atom parity up to the C_{12} chain length (see Figure 9 of ref 7a). Beyond C_{12} chain length, there is a trend reversal—odd biscarbamates show higher spherulitic growth rate than the corresponding even biscarbamates. For example, the spherulite growth rate of C_7C_6 is 100 $\mu\text{m}/\text{s}$, while that of C_8C_6 is about 120 $\mu\text{m}/\text{s}$. A similar trend is seen in the case of the $C_{11}C_6/C_{12}C_6$ pair where the growth rate of $C_{11}C_6$ is 55 $\mu\text{m}/\text{s}$ and that of $C_{12}C_6$ is about 65 $\mu\text{m}/\text{s}$.

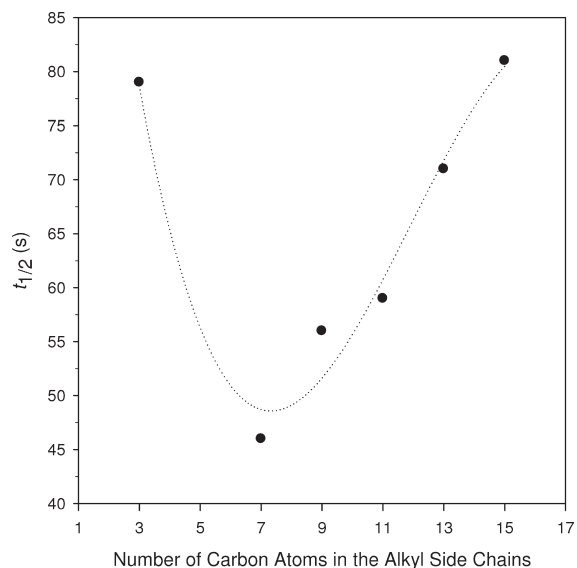


Figure 11. Change of half crystallization time, $t_{1/2}$, as a function of number of carbon atoms in the alkyl side chains. The dotted curve serves to guide the eyes.

However, the spherulite growth rate of $C_{15}C_6$ is higher (50 $\mu\text{m}/\text{s}$) than that of $C_{16}C_6$ biscarbamate ($\sim 30 \mu\text{m}/\text{s}$).

Rate of Isothermal Crystallization. Isothermal crystallization studies of the samples were performed on the DSC and analyzed using the Avrami approach to investigate the differences in the crystallization rates between the odd and even numbers of carbon atoms in the alkyl side chains. Figure 9 shows the fractional heat of fusion (α) as a function of time for three representative odd-biscarbamates with extreme and intermediate alkyl side chain length, namely, C_3C_6 , C_7C_6 , and $C_{15}C_6$, as well as C_8C_6 . Results for the other biscarbamates studied in this series are not shown in this figure for the sake of clarity. As noted with the spherulite size and spherulite growth rate variation, we see a much slower rate of crystallization for the biscarbamates with extreme alkyl side chain length compared to those having intermediate side chain length. It is seen from the inset in Figure 9 that biscarbamate with the shortest side chain length (C_3C_6) requires a longer induction period for the commencement of crystallization, while those with longer side chain length (e.g., $C_{15}C_6$) start crystallization immediately after reaching the desired temperature. However, the faster rate of initial crystallization of longer chain biscarbamates slows down over time with the progress of crystallization, and the initial slower crystallization rate of shorter chain length biscarbamate is overcome after a certain time period during their isothermal crystallization. Along this series of biscarbamates, C_7C_6 has the shortest induction time and narrowest peak time range (1.9 min) compared to those of the extreme chain length biscarbamates (9 min for C_3C_6 and $C_{15}C_6$, respectively) indicating the fastest crystallization rate. It is also seen that C_7C_6 of the odd series and C_8C_6 show very similar crystallization rates.

Figure 10 shows the plots of $\ln\{-\ln[1 - X(t)]\}$ versus $\ln t$ for biscarbamates crystallized isothermally at their respective crystallization temperatures with a linear relationship between these two parameters. The results derived from the Avrami equation are given in Table 1. It is seen that the exponent n is significantly smaller than 3, varying from 1.6 to 2.6 depending on the side chain length. A value of n from less than 3 shows that the crystallization (nucleation and growth) is not truly three-dimensional.

Table 2. Infrared Data for H-Bonded N—H and C=O Stretching Bands of Biscarbamates with an Odd Number of Carbon Atoms in the Alkyl Side Chains

ID	H-bonded N—H			H-bonded C=O		
	frequency (cm ⁻¹)	intensity	fwhm	frequency (cm ⁻¹)	intensity	fwhm
C ₃ C ₆	3326	25.8	26.6	1681	43.6	26.4
C ₇ C ₆	3320	26.9	17.1	1681	47.7	16.7
C ₉ C ₆	3320	25.6	18.9	1682	52.4	21.1
C ₁₁ C ₆	3319	27.8	19.0	1682	54.1	22.0
C ₁₃ C ₆	3318	25.9	19.5	1682	57.2	21.4
C ₁₅ C ₆	3318	25.4	19.7	1682	58.7	24.6

Table 3. Infrared Data for Symmetric (ν_s) and Asymmetric (ν_{as}) Stretching Bands of CH₂ Groups in Biscarbamates with Different Alkyl Side Chains

ID	asymmetric		symmetric	
	frequency (cm ⁻¹)	intensity	frequency (cm ⁻¹)	intensity
C ₃ C ₆	2938	42.5	2858	28.6
C ₇ C ₆	2921	40.5	2856	27.0
C ₉ C ₆	2918	40.5	2853	27.0
C ₁₁ C ₆	2917	40.5	2851	27.0
C ₁₃ C ₆	2916	40.5	2851	27.0
C ₁₅ C ₆	2915	40.5	2850	27.0

This is evident from the eaves trough-like growth of the spherulites seen for C₁₃C₆ in Figure 7, which shows the smallest value of n . At the extreme chain lengths, both C₃C₆ and C₁₅C₆ show the same value of n , while the highest value of 2.6 is seen for C₇C₆. The Avrami exponent obtained from the slope of the curves in Figure 10 was used to calculate the $t_{1/2}$ (time required for 50% crystallization) for the respective biscarbamates according to eq 4. The variation in $t_{1/2}$ values with alkyl side chain length is shown in Figure 11. It is seen that C₇C₆ has the lowest $t_{1/2}$ value and hence the highest crystallization rate among this series, while the biscarbamates with extreme side chain lengths have higher $t_{1/2}$ and consequently lower crystallization rate. This observation is in good agreement with their spherulite size and spherulitic growth kinetics. The $t_{1/2}$ values of C₇C₆ and C₁₁C₆ are 46 and 59 s, respectively, while that of C₈C₆ and C₁₂C₆ studied earlier were only 8 and 40 s, respectively. Note that although the spherulite growth (shown in Figure 8) stops at a certain time due to impingement, crystallization continues and hence the $t_{1/2}$ values are higher. Comparison of the $t_{1/2}$ values of two biscarbamates containing successive odd and even numbers of carbon atoms shows that biscarbamate with an even number of carbon atoms shows faster crystallization rate than that of the odd biscarbamate with comparable side chain length.

Infrared Spectroscopy. Infrared spectroscopy was performed with samples prepared with two different protocols, i.e., by quenching and slow cooling. There was no significant difference in the spectral profiles of the slow-cooled and quenched samples which indicates that the type of intermolecular interactions of these molecules seemed to be independent of sample preparation protocol (quenching or slow cooling), and the data presented here are of slow-cooled samples. The spectral data

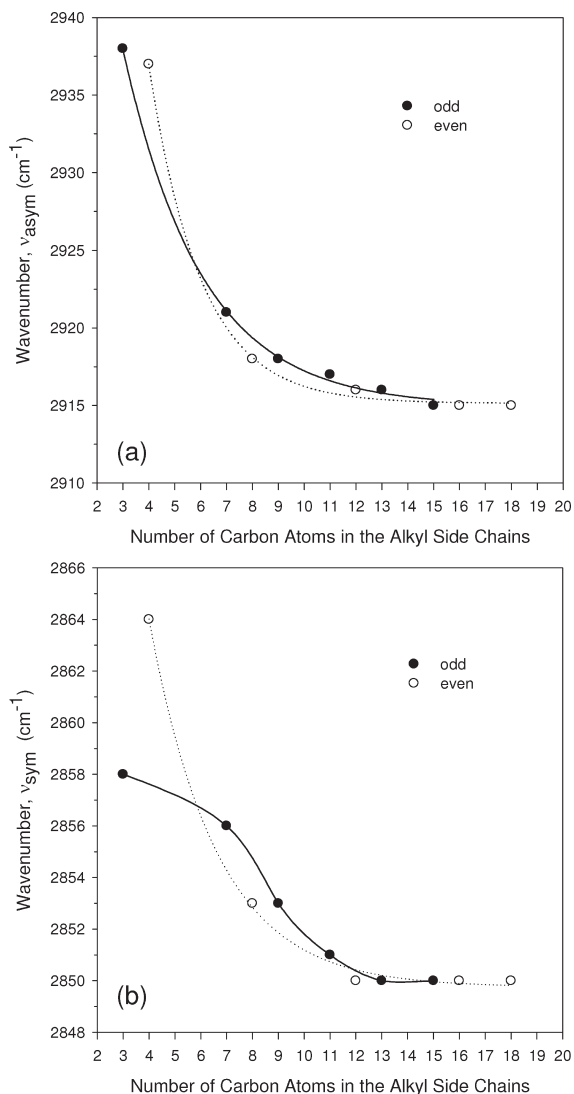


Figure 12. Variation of (a) asymmetric and (b) symmetric CH₂ stretching vibration frequencies of biscarbamates with alkyl side chain length. The curves serve to guide the eyes.

corresponding to N—H, C=O, and CH₂ groups are summarized in Tables 2 and 3. The full width at half-maximum of the peaks (fwhm) were calculated after normalizing them with respect to the C=O stretching band of the carbonyl group which was the most intense and appeared at the same frequency for all compounds. (We did not choose the CH stretching vibrations of CH₂ groups for such normalization since both the intensity and absorption frequency of this peak changed with the variation in the alkyl side chain length.)

Biscarbamates of this series show a H-bonded N—H stretching band at around 3319 cm⁻¹ except for C₃C₆ which appears at 3326 cm⁻¹. The C=O stretching band of these molecules appears at 1681 cm⁻¹ without any significant shift in position with respect to side chain length. Two other strong absorption bands corresponding to the symmetric and asymmetric stretching vibrations of CH₂ groups were observed at ~2853 and 2920 cm⁻¹, respectively. A weak band at 2953 cm⁻¹ and a very weak band at 2877 cm⁻¹ corresponding to the C—H asymmetric and symmetric vibrations of the terminal CH₃ groups were also

observed. These weak bands diminish with the increased contribution of the CH_2 groups as the alkyl side chain length increases. Because of the difference in their bond order, the N—H stretching mode was found to be more susceptible to the change in intermolecular interactions than that of the C=O group. A similar trend was seen with the symmetric and asymmetric C—H vibrations where asymmetric vibrations were found to be more susceptible. The N—H stretching band of C_3C_6 appears at 3326 cm^{-1} and shifts to 3318 cm^{-1} for C_{15}C_6 , while that of C_4C_6 appears at 3321 cm^{-1} and shifts to 3316 cm^{-1} for C_{16}C_6 . However, the C=O bands appear at 1682 cm^{-1} for all of these molecules of both the odd and even numbered series. It is seen from Table 2 that the full width at half maxima (fwhm) of the H-bonded N—H and C=O bands significantly decrease with the increase in alkyl side length from C_3 to C_7 . Beyond C_7 , fwhm increases, although marginally, with further increase in the alkyl side chain length. Such variation in the half width is indicative of enhanced molecular interactions and was attributed to the crystalline order of simple polyurethanes.³⁹ Reduction in half width thus indicates an increase in crystalline order in the present case. Thus, the lowest half width of the H-bonded N—H and C=O bands for C_7 indicates the highest crystalline order among the biscarbamates of this series studied here. Note that this molecule also showed the highest value of the Avrami exponent n .

The variation of van der Waals interaction as a function of the alkyl side chain length is reflected in the shift of asymmetric (ν_{as}) and symmetric (ν_s) absorption band positions. The decrease of ν_{as} and ν_s with the alkyl side chain length is shown in Figure 12. For C_3 , ν_{as} and ν_s appear at 2938 and 2858 cm^{-1} , while they shift to 2915 and 2850 cm^{-1} , respectively, for C_{15} . The shift to lower wavenumber with side chain length indicates the stronger interaction and hence more organization of the alkyl groups via van der Waals forces. Between the two complementary attractive forces, hydrogen bonding dominates over van der Waals interactions when the alkyl side chain length is short (C_3 – C_7), and the packing of the short alkyl chains would also be less efficient due to the CH_3 end group. With an increase in the alkyl side chain length (C_9 – C_{15}), the contribution of the hydrogen bonds remains the same, while van der Waals interactions become more significant leading to enhanced packing of the alkyl side chain length. A similar trend was seen with the biscarbamate with an even number of carbon atoms in the alkyl side chain length.

CONCLUSIONS

We discussed the crystallization behavior and morphology of a series of homologous biscarbamate molecules with alkyl side chains of different carbon atom parity. DSC analysis showed these are highly crystalline, with a single melt transition, consistent with a lack of polymorphic transitions. The melting temperatures of C_xC_6 molecules with an odd versus even number of carbon atoms in the alkyl side chains show an odd–even alternation. Biscarbamates with an odd number of carbon atoms show higher melting temperatures than the even-numbered biscarbamates, which is in contrast to the thermal properties of *n*-alkanes. This is rationalized on the basis of the *anti* and *syn* conformations of the terminal C— CH_3 bonds in even and odd numbered *n*-alkanes and such conformations with respect to C—O and C— CH_3 bonds in biscarbamates. Optical microscopy reveals that carbon atom parity in alkyl side chains influences the extent of packing of these molecules leading to spherulitic morphology. C_4C_6 biscarbamate does not show any spherulitic morphology,

whereas C_3C_6 forms well-defined spherulites upon crystallization from the melt. The spherulite size increases with alkyl side chain length, reaching a maximum at a certain length, and then decreases with further increase. Along this series of molecules, a maximum in spherulite size and spherulite growth rate is seen for C_7C_6 (odd series) and C_8C_6 (even series) biscarbamates. Similar behavior is seen with the rate of crystallization also. Using the Lennard-Jones function, the van der Waals interaction for each $\text{CH}_2 \cdots \text{CH}_2$ pair⁴⁰ at a distance of 3.5 \AA is about -0.5 kcal/mol . The typical N—H \cdots O hydrogen bond interaction energy is about -3.0 kcal/mol . Thus, with an alkyl side chain length of C_7 , the van der Waals energy (-3.5 kcal/mol) and the hydrogen bond energy equally contribute to the interactions, and the former becomes more significant with longer alkyl side chains. Both van der Waals and hydrogen bond interactions are balanced with a side chain length of C_7 with the odd series and with C_8 in the case of even carbon atom parity. Hence the length of the alkyl side chain, carbon atom parity in the alkyl side chains, and sample preparation protocol (i.e., quenching versus slow cooling) play an important role in the morphology of these molecules. In this series of homologous biscarbamates bearing two hydrogen-bonding moieties, the energy of interaction due to hydrogen bonds remains constant. However, the van der Waals interaction increases with the alkyl side chain length. Thus, the crystallinity and morphology of the hydrogen bond mediated self-assembled system are controlled by the van der Waals forces between the alkyl side chains.

ASSOCIATED CONTENT

S Supporting Information. DSC curves of C_3C_6 and C_4C_6 biscarbamates and a table of melting temperatures. This material is available free of charge via the Internet at <http://pubs.acs.org>.

AUTHOR INFORMATION

Corresponding Author

*E-mail: sundar@carleton.ca.

ACKNOWLEDGMENT

Financial support from Natural Sciences and Engineering Research Council of Canada (NSERC) is gratefully acknowledged.

REFERENCES

- (a) Lehn, J.-M. *Supramolecular Chemistry*; VCH: Germany, 1995. (b) *Supramolecular Assembly via Hydrogen Bonds II: Structure and Bonding*, 111; Mingos, D. M. P., Ed. (St. Edmund Hall, Oxford, UK); Springer-Verlag: Berlin, Heidelberg, NY, 2004. (c) Ikeda, M.; Nobori, T.; Schmutz, M.; Lehn, J.-M. *Chem.—Eur. J.* **2005**, *11*, 662.
- (2) Special Issue on Supramolecular Chemistry and Self-Assembly. Service, R. F.; Szuromi, P.; Uppenbrink, J. *Science* **2002**, *295*, 2395.
- (3) (a) Tew, G. N.; Scott, R. W.; Klein, M. L.; Degrado, W. F. *Acc. Chem. Res.* **2010**, *43*, 30. (b) Horne, W. S.; Gellman, S. H. *Acc. Chem. Res.* **2008**, *41*, 1399. (c) Gellman, S. H. *Acc. Chem. Res.* **1998**, *31*, 173. (d) Hill, D. J.; Mio, M. J.; Prince, R. B.; Hughes, T. S.; Moore, J. S. *Chem. Rev.* **2001**, *101*, 3893.
- (4) (a) Sanford, A. R.; Yamato, K.; Yang, X.; Yuan, L.; Han, Y.; Gong, B. *Eur. J. Biochem.* **2004**, *271*, 1416. (b) Yang, X.; Martinovic, S.; Smith, R. D.; Gong, B. *J. Am. Chem. Soc.* **2003**, *125*, 9932. (c) Archer, E. A.; Gong, H.; Krische, M. J. *Tetrahedron* **2001**, *57*, 1139.
- (5) Zimmerman, S. C.; Corbin, P. S. *Struct. Bonding (Berlin)* **2000**, *94*, 63.

- (6) (a) Moniruzzaman, M.; Goodbrand, B.; Sundararajan, P. R. *J. Phys. Chem. B* **2003**, *107*, 8416. (b) Moniruzzaman, M.; Sundararajan, P. R. *Langmuir* **2005**, *21*, 3802.
- (7) (a) Khanna, S.; Moniruzzaman, M.; Sundararajan, P. R. *J. Phys. Chem. B* **2006**, *110*, 15251. (b) Khanna, S.; Khan, M. K.; Sundararajan, P. R. *Langmuir* **2009**, *25*, 13183.
- (8) Tao, F.; Bernasek, S. L. *Chem. Rev.* **2007**, *107*, 1408.
- (9) (a) Badea, E.; Gatta, G. D.; D'Angelo, D.; Brunetti, B.; Rečková, Z. *J. Chem. Thermodyn.* **2006**, *38*, 1546. (b) Duer, M. J.; Roper, C. *Phys. Chem. Chem. Phys.* **2003**, *5*, 3034.
- (10) (a) Pistolis, G.; Andreopoulou, A. K.; Malliaris, A.; Kallitsis, J. K. *J. Phys. Chem. B* **2005**, *109*, 11538. (b) Meister, A.; Drescher, S.; Garamus, V. M.; Karlsson, G.; Graf, G.; Dobner, B.; Blume, A. *Langmuir* **2008**, *24*, 6238. (c) Stals, P. J. M.; Smulders, M. M. J.; Martín-Rapún, R.; Palmans, A. R. A.; Meijer, E. W. *Chem.—Eur. J.* **2009**, *15*, 2071.
- (11) (a) Kikkawa, Y.; Koyama, E.; Tsuzuki, S.; Fujiwara, K.; Kanesato, M. *Langmuir* **2010**, *26*, 3376. (b) Tong, W.; Wei, Y.; Armbrust, K. W.; Zimmt, M. B. *Langmuir* **2009**, *25*, 2913.
- (12) Boese, R.; Weiss, H.-C.; Bläser, D. *Angew. Chem., Int. Ed.* **1999**, *38*, 988.
- (13) (a) Šepelj, M.; Lesac, A.; Baumeister, U.; Diele, S.; Bruce, D. W.; Hamersák, Z. *Chem. Mater.* **2006**, *18*, 2050. (b) Mather, P. T.; Jeon, H. G.; Han, C. D.; Chang, S. *Macromolecules* **2002**, *35*, 1326. (c) Mizuno, M.; Hirai, A.; Matsuzawa, H.; Endo, K.; Suhara, M.; Kenmotsu, M.; Han, C. D. *Macromolecules* **2002**, *35*, 2595.
- (14) Fernández, C. E.; Bermúdez, M.; Muñoz-Guerra, S.; León, S.; Versteegen, R. M.; Meijer, E. W. *Macromolecules* **2010**, *43*, 4161.
- (15) Briard, A.-J.; Bouroukba, M.; Petitjean, D.; Dirand, M. *J. Chem. Eng. Data* **2003**, *48*, 1574.
- (16) Tao, F.; Goswami, J.; Bernasek, S. L. *J. Phys. Chem. B* **2006**, *110*, 4199.
- (17) Morishige, K.; Kato, T. *J. Chem. Phys.* **1999**, *111*, 7095.
- (18) (a) Tao, F.; Bernasek, S. L. *Langmuir* **2007**, *23*, 3513. (b) Wintgens, D.; Yablon, D. G.; Flynn, G. W. *J. Phys. Chem. B* **2003**, *107*, 173.
- (19) (a) Kim, K.; Plass, K. E.; Matzger, A. J. *J. Am. Chem. Soc.* **2005**, *127*, 4879. (b) Asha, S. K.; Kavita, K.; Das, P. K.; Ramakrishnan, S. *Chem. Mater.* **1999**, *11*, 3352. (c) Aoki, K.; Kudo, M.; Tamaoki, N. *Org. Lett.* **2004**, *6*, 4009.
- (20) (a) Goel, M.; Jayakannan, M. *J. Phys. Chem. B* **2010**, *114*, 12508. (b) Wei, Y.; Kannappan, K.; Flynn, G. W.; Zimmt, M. B. *J. Am. Chem. Soc.* **2004**, *126*, 5318.
- (21) Atwell, G. J.; Fan, J.-Y.; Tan, K.; Denny, W. A. *J. Med. Chem.* **1998**, *41*, 4744.
- (22) Martinek, T. W.; Klass, D. L. U.S. Patent 3,335,139, 1967.
- (23) Chueca, A.; Baron, M.; Lopez, G. J. *Photosynthesis Proceedings International Congress, 5th*; Akoyunoglou, G., Ed.; Balaban Int. Sci. Serv.: Philadelphia, PA; 1981; p 555; *Chem Abstr.* **1981**, *97*, 50917.
- (24) Papot, S.; Bachmann, C.; Combaud, D.; Gesson, J.-P. *Tetrahedron* **1999**, *55*, 4699.
- (25) Xu, S.; Chen, M.; Yao, Y.; Zhang, Z.; Jin, T.; Huang, Y.; Zhu, H. *J. Controlled Release* **2008**, *130*, 64.
- (26) Anderson, W. K.; Mach, R. H. *J. Med. Chem.* **1987**, *30*, 2109.
- (27) Chambers, J.; Reese, C. B. *Brit. Polym. J.* **1977**, *9*, 41.
- (28) Matzger, A. J.; Kim, K. *Polym. Mater. Sci. Eng.* **2003**, *89*, 825.
- (29) (a) Steichele, K. Belg. Patent 882,922, 1980: *Chem. Abstr.* **1980**, *94*, 66768d. (b) Saka, K.; Noda, K. *Jpn. Kokai Tokkyo Koho JP* **62** 179584, 1987: *Chem. Abstr.* **1987**, *108*, 39820r. (c) Tanaka, K.; Kano, Y.; Yoshida, K. *Jpn. Kokai Tokkyo Koho JP* **63** 248 894, 1988: *Chem. Abstr.* **1988**, *110*, 79137w. (d) Kinoshita, H.; Sekiya, M.; Mishima, M. *Eur. Pat. EP* **274 756**, 1988: *Chem. Abstr.* **1988**, *109*, 233979k.
- (30) Rohr, W.; Franke, A.; Giertz, H.; Amann, A. *Brit Patent* **1,396,523**, 1975.
- (31) D'Silva, T. D. J. U.S. Patent 4,400,389, 1983.
- (32) (a) *Jpn. Kokai Tokyo Koho JP* **58** 201 758, 1983; *Chem Abstr.* **1983**, *100*, 174289z. (b) Tanaka, T.; Yoshitomi, T.; Hanada Y.; Ohashi, M.; Takeda, Y. *Jpn. Kokai Tokkyo Koho JP* **62** 090 289, 1987; *Chem Abstr.* **1987**, *107*, 208963. (c) Goodbrand, B.; Boils, D.; Sundararajan, P. R.; Wong, R.; Malhotra, S. U.S. Patent 6,187,082, 2001.
- (33) Khan, M. K.; Sundararajan, P. R. *J. Phys. Chem. B* **2008**, *112*, 4223.
- (34) Goodbrand, B.; Boils, D.; Sundararajan, P. R.; Wong, R. U. S. Patent 6,414,051, 2002.
- (35) (a) Avrami, M. *J. Chem. Phys.* **1939**, *7*, 1103. (b) Avrami, M. *J. Chem. Phys.* **1941**, *9*, 177.
- (36) Klug, H. P.; Alexander, L. E. *X-Ray Diffraction Procedures*; John Wiley & Sons: New York, 1954.
- (37) Alimova, L. L.; Atovmyan, E. G.; Filipenko, O. S. *Kristallografiya* **1987**, *32*, 97.
- (38) (a) McKiernan, R. L.; Heintz, A. M.; Hsu, S. L.; Gido, S. P.; Penelle, J. *Polym. Mater. Sci. Eng.* **2001**, *84*, 416. (b) Saito, Y.; Nansai, S.; Kinoshita, S. *Polym. J.* **1972**, *3*, 113.
- (39) Coleman, M. M.; Lee, K. H.; Skrovanek, D. J.; Painter, P. C. *Macromolecules* **1986**, *19*, 2149.
- (40) Abe, A.; Jernigan, R. L.; Flory, P. J. *J. Am. Chem. Soc.* **1966**, *88*, 631.